AUT Journal of Electrical Engineering

AUT J. Electr. Eng., 55(2) (2023) 145-160
DOI: 10.22060/eej.2023.22529.5547

Exploring the Potential of Elliptical Metasurfaces for Decoupling and Cloaking of Tightly Spaced and Interleaved Patch Array Antennas in 5G Applications

Reza Masoumi, Robab Kazemi*

Faculty of Electrical and Computer Engineering, University of Tabriz, Tabriz, Iran

ABSTRACT: This study investigates the effectiveness of mantle cloaking in isolating two densely packed patch antenna arrays with close operating frequencies. The cloak used is an elliptical metasurface consisting of vertical strips on a thin dielectric layer. This metasurface cloak reduces strong mutual coupling between adjacent elements of co-planar arrays by exhibiting capacitive reactance at the desired operating frequency and eliminating the inductive reactance caused by induced currents from adjacent patches. As a result, the elements of the two arrays become invisible to each other. To enable beam steering, the size of the patches is reduced by 34% through the addition of two slots on the resonant edges. The performance of the arrays is evaluated based on impedance matching, isolation, gain, radiation patterns, and efficiency. The results indicate that the addition of the cloak increased array efficiency by 35% compared to the uncloaked case. Additionally, the isolation between elements improved by over 15 dB at the operating frequency. The radiation patterns in the cloaked case closely resembled those of isolated arrays with a similarity of 98% which is calculated using the Pearson Correlation Method (PCM). However, in the cloaked case, there was a slight decrease in antenna gain by 0.7 dB and 0.5 dB for Array I and Array II, respectively. Furthermore, the sidelobe levels increased by 0.7 dB compared to isolated arrays. These findings confirm that the designed metasurface cloak effectively replicated the radiation characteristics of closely spaced arrays, resembling those of isolated arrays.

Review History:

Received: Jul. 04, 2023
Revised: Aug. 12, 2023
Accepted: Sep. 12, 2023
Available Online: Oct. 01, 2023

Keywords:

Decoupling
Mantle cloaking
Elliptical metasurface
Beam steering
Patch antenna

1- Introduction

Pendry [1] first introduced the concept of "electromagnetic cloaking" using metamaterials to render a metal cylinder invisible to incoming waves. He used the transformation optics theory to design a cloak that was independent of the shape and material of the object being cloaked. The copper cylinder was hidden within a metamaterial cloak, resulting in the world's first practical manifestation of such a cloak. However, mantle cloaking, which involves cloaking through a surface, was later introduced in [2]. This approach quickly gained popularity over the bulky metamaterial cloaks due to its lightweight nature, ease of manufacturing, low cost, and adaptable design. Mantle cloaking has primarily been used to hide passive objects from emitting devices, such as radars [2]. These cloaking techniques involve reducing and canceling the scattering from the objects. In addition, multi-layer mantle cloaks have been developed to hide larger objects with complex structures [3]. Furthermore, polarization-sensitive metasurfaces have been developed to exhibit different cloaking behaviors for incident TE and TM waves [4].

Cloaking active devices and antennas is a more intricate process compared to passive components, as it can affect their impedance matching and radiation characteristics. The cloak covering an antenna must preserve its matching and radiation capabilities and conceal it from nearby radiators. Active device cloaking has been limited to the decoupling of simple antenna arrays including non-planar arrays of cylindrical and printed monopole antennas [5, 6] as well as Yagi-Uda antennas [7] so far. However, these antennas have a relatively low gain, rendering them unsuitable for advanced communication systems such as 5G and 6G mobile networks.

Nonlinear cloaks, which use metasurfaces loaded with active devices and diodes, operate in on/off cloaking mode based on input power [8-10] or incident wave [11, 12]. However, these cloaks have only been successful in cloaking simple monopole antennas and loaded active devices have limited bandwidth. These issues need to be addressed to make nonlinear cloaks more practical.

Several techniques, including defected ground structure (DGS) [13], parasitic elements [14], electromagnetic band-gap structures [15], polarization conversion isolators [16], and metamaterial-based DGSs [17], have been utilized to achieve high decoupling and inter-element isolation of antennas. However, these methods are limited by their large size, multilayer structure, and high manufacturing complexity and cost.

This paper presents a new approach that employs elliptical mantle cloaks to isolate two closely spaced interleaved

*Corresponding author's email: r.kazemi@tabrizu.ac.ir

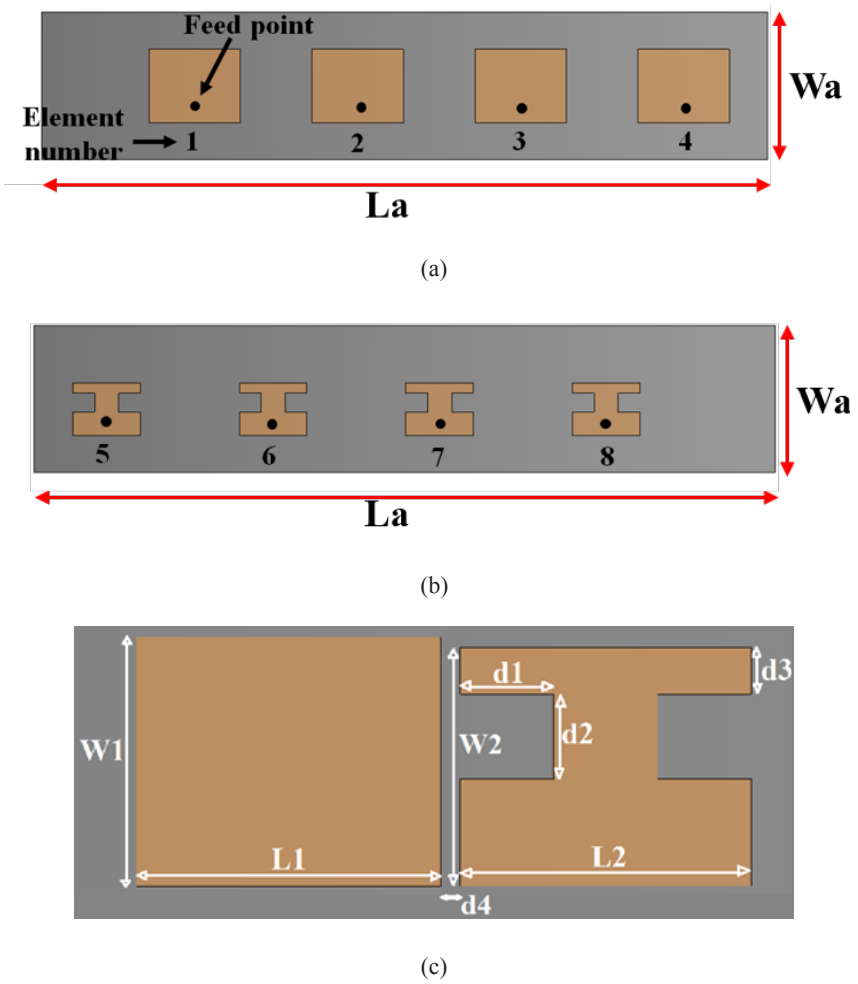

Fig. 1. a) Array I, b) Array II, c) dimensions of the elements of two arrays

patch antenna arrays. The edge-to-edge spacing between the elements has been significantly reduced to $\lambda/100$ (0.1 mm), which is much smaller than previous arrays. Additionally, the size of the second array has been reduced by incorporating two rectangular slots at the edges, resulting in a spacing between the elements of less than half-wavelength ($\lambda/2$). This enables ±90° full-range beam steering without any grating lobes.

Using the proposed cloaking structure, the impedance matching and isolation between the elements of the arrays have been improved, and the radiation characteristics of the antennas are almost the same as those of the isolated single element. This design is a good candidate for the implementation of compact communication antennas.

2- Design Process

2- 1- Investigation of the characteristics of the patch arrays in isolated and uncloaked cases

In this study, we examine two linear arrays of microstrip patch antennas illustrated in Fig. 1. These arrays, fed by coaxial cables, each comprise four patch antennas and are fabricated on a resin substrate with a thickness of 0.2 mm, ε_r = 4, and tanδ = 0.01. The elements of the first array (Array I) are conventional rectangular patch antennas operating at 27.5 GHz, while those of the second array (Array II) are modified patch antennas with two slots at the edges and operate at 26.5 GHz.

The slots of the elements of Array II cause the resonance frequency of the patch to be shifted down; as a result, its dimensions are reduced by 34% compared to the conventional patch. This size reduction results in the inter-element spacing of both arrays being less than $\lambda/2$, enabling them for beam steering in phased array applications. Dimensions of the two arrays are summarized in Table 1.

The two arrays of Fig. 1(a) and 1(b) are separately simulated in CST Microwave Studio software and their reflection coefficients are shown in Fig. 2.

Then, the elements of the two arrays are densely interleaved without increasing the antenna aperture, as shown in Fig. 3. The edge-to-edge spacing of the patches is $\lambda/100$ (0.1 mm) and the inter-element spacing of the arrays I and II is L_s = 5.56 mm, which is 0.505 λ_1 and 0.49 λ_2, respectively, where λ_1 and λ_2 are the wavelengths at the operating frequencies of

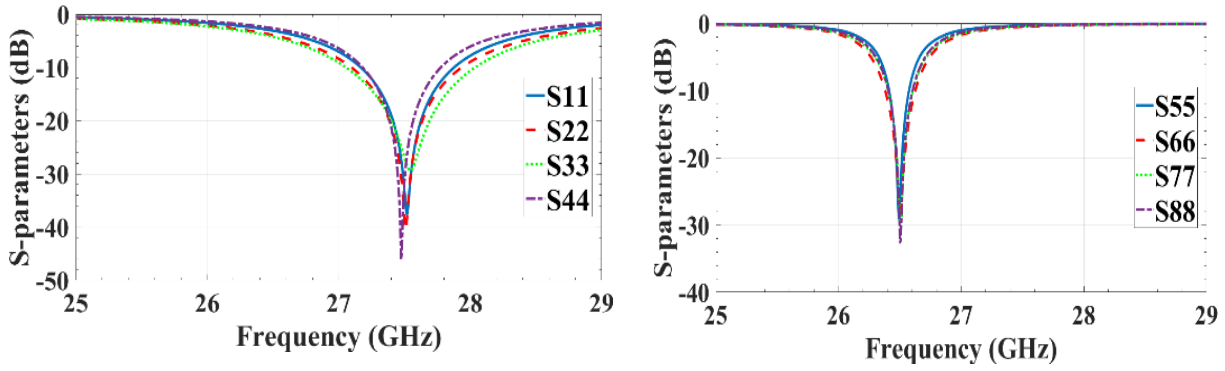

(a) (b)

Fig. 2. Reflection coefficients of elements in the isolated configuration. a) Array I, b) Array II

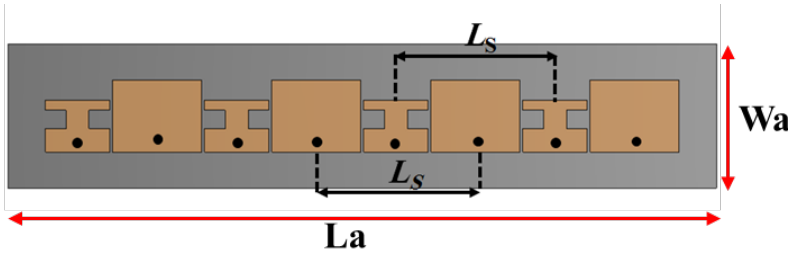

Fig. 3. Tightly spaced interleaved two uncloaked arrays

two arrays.

Fig. 4 shows a comparison of the mutual coupling between the central elements of two arrays, both in isolated and interleaved uncloaked configurations. As expected, the closely spaced interleaved uncloaked arrays exhibit strong coupling (S_{37}), leading to changes in the input impedances of the elements and a decline in their matching. The reflection coefficients of the elements in both arrays are depicted in Fig. 5. It can be observed that the matching of the elements in the interleaved uncloaked arrays is degraded compared to the isolated cases of Fig. 2.

To mitigate the negative effects of strong coupling, elliptical metasurface mantle cloaks are implemented to cover all of the elements in the interleaved uncloaked arrays. These cloaks are specifically designed for each array element and are able to cancel out the scattering of one array antenna at the operating frequency of the other array. Mathieu's odd and even functions can be utilized to compute the incident and scattered fields of a metallic elliptic cylinder (a cylinder with an elliptic cross-section). To analyze patch antennas, we employed this theory by approximating the thin metallic rectangular patch as a metallic elliptic cylinder with a minor diameter of b_1. As the metal patch is exceedingly thin, we set the minor diameter of the cylinder to zero. The 3D and 2D configurations of both the patch and model structure are illustrated in Fig. 6.

Modeling infinitely extended cylinders simplifies the 3D scattering problem by reducing it to a 2D problem. However, since infinitely extended cylinders do not exist in nature, it is necessary to derive approximate solutions for cylindrical structures with finite lengths. This is the first step toward analyzing more realistic structures.

To model the patch antenna, we initially used an infinite elliptical cylinder. The major diameter of the cylinder represents the width of the metal patch, while the minor diameter represents the thickness of the patch (which tends to zero). In deriving the analytical formulas, we accurately consider the width of the patch without any approximation. The only approximation made is for the finite case formulation, where the length of the patch is finite compared to the infinite length of the cylinder.

The scattering behavior of dipoles/monopoles that

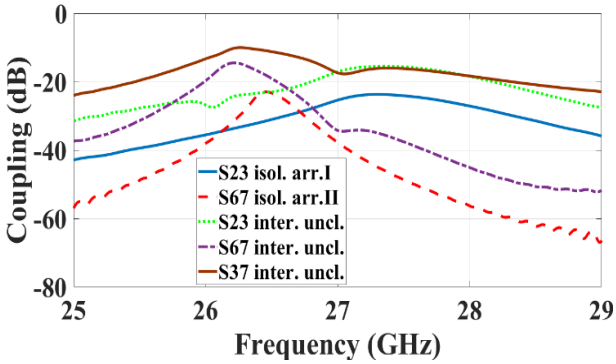

Fig. 4. Mutual coupling between the central patches of two arrays in the isolated and interleaved uncloaked configurations

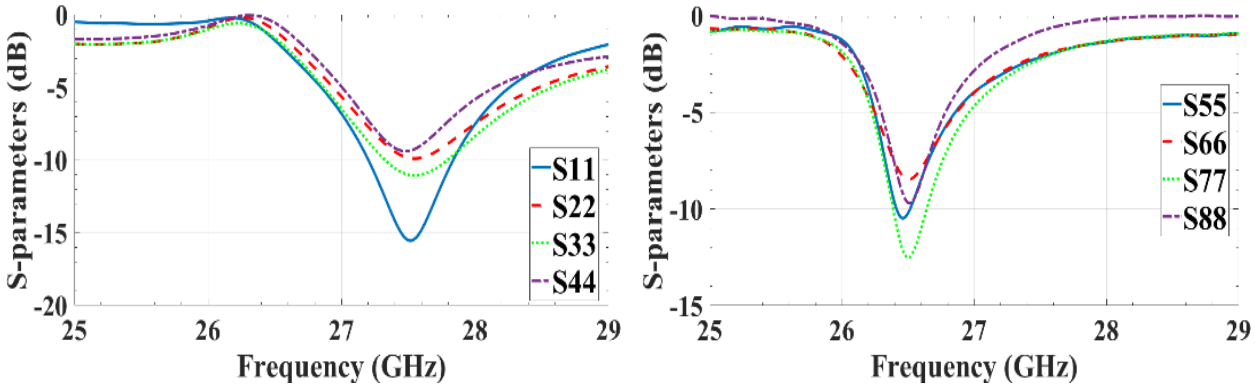

(a) (b)

Fig. 5. Reflection coefficients of elements in the interleaved uncloaked configuration. a) Array I, b) Array II

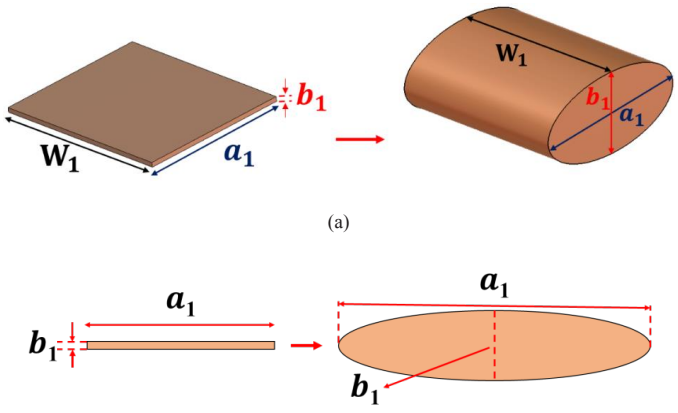

(a)

(b)

Fig. 6. a) 3D and b) 2D views of a thin metallic rectangular patch approximated by a metallic elliptic cylinder with a minor diameter (b_1) of zero

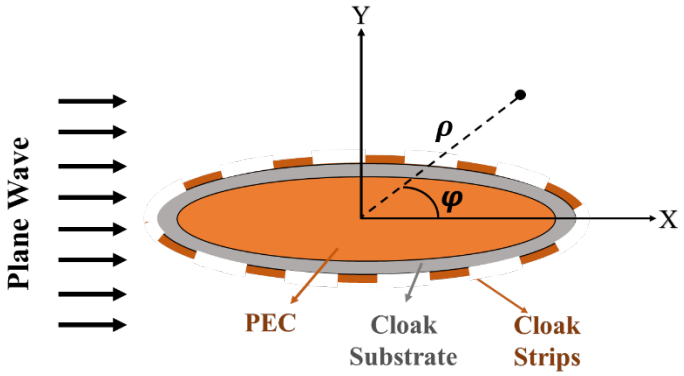

Fig. 7. Scattering of an incident plane wave by a cloaked infinite PEC cylinder with an elliptical cross-section

resemble infinitely long cylinders has been determined by formulating incident, transmitted, and scattered fields. When the cylinder has an elliptical cross-section, the problem is analyzed using the separation of variables method and the widely-known Mathieu angular and radial equations. The geometry of the problem is depicted in Fig. 7.

In this case, the incident and scattered electric and magnetic fields are expressed in terms of Mathieu's odd and even functions in elliptical coordinates [18], as follows:

$$E_z^i = \sqrt{8\pi}\sum_n j^{-n}\frac{J_{pm}(q_0,u,n)}{N_{pm}(q_0,n)} \times S_{pm}(q_0,v,n)S_{pm}(q_0,\varphi,n) \quad (1)$$

$$E_z^s = \sqrt{8\pi}\sum_n j^{-n}\alpha_{pm}^{(n)}H_{pm}^{(1)}(q_0,u,n) \times S_{pm}(q_0,v,n)S_{pm}(q_0,\varphi,n) \quad (2)$$

where $J_{pm}(q_0,u,n)$ is the radial Mathieu function of the first kind, $S_{pm}(q_0,v,n)$ is the angular Mathieu function, $N_{pm}(q_0,n)$ is the normalization constant, u is the radial distance, v is the angular coordinate, $q_0 = k_0^2\frac{F^2}{4}$, $H_{pm}^{(1)}(q_0,u,n)$ is the radial Mathieu function of the third kind indicating the outgoing wave, and $\alpha_{pm}^{(n)}$ are the unknown coefficients.

Having E-fields, the magnetic incident and scattered fields can be determined using Maxwell's equations. By applying the boundary conditions at the interface of the metal cylinder and the covering dielectric (cloak substrate), the unknown coefficients, $\alpha_{pm}^{(n)}$, are calculated and the total scattering cross-section (SCS) can be determined as:

$$\sigma_{total} = \frac{1}{2\pi}\int_0^{2\pi}\sigma_{2D}(v)dv \quad (3)$$

where

$$\sigma_{2D} = \lambda\left|\sum_n \sqrt{8\pi}j^{-2n}\alpha_{pm}^{(n)}S_{pm}(q_0,v,n).S_{pm}(q_0,\varphi,n)\right|^2 \quad (4)$$

To eliminate the total scattering, the scattering coefficient of each mode, $\alpha_{pm}^{(n)}$, is set to zero. Then, the equivalent surface reactance required to cancel the scattering of each mode is determined. The calculation of the required surface reactance to cancel the scattering of the first mode, X_{opt}, which significantly contributes to the scattering of the elliptic cylinder, is obtained in a closed form using the quasi-static approximation. The details of the formulation of X_{opt} are provided in the manuscript and utilized in the current study to compute the parameters of the metasurface cloak, specifically parallel metal strips.

When a TM mode is used for illumination, the SCS of a finite cylinder with a length L (3D case) can be connected to the SCS of an infinite cylinder (2D case) as follows [19]:

$$\sigma_{total} = \frac{1}{4\pi}\int\sigma_{3D}d\Omega = \frac{1}{4\pi}\iint\sigma_{3D}\sin\theta d\theta d\varphi \quad (5)$$

where

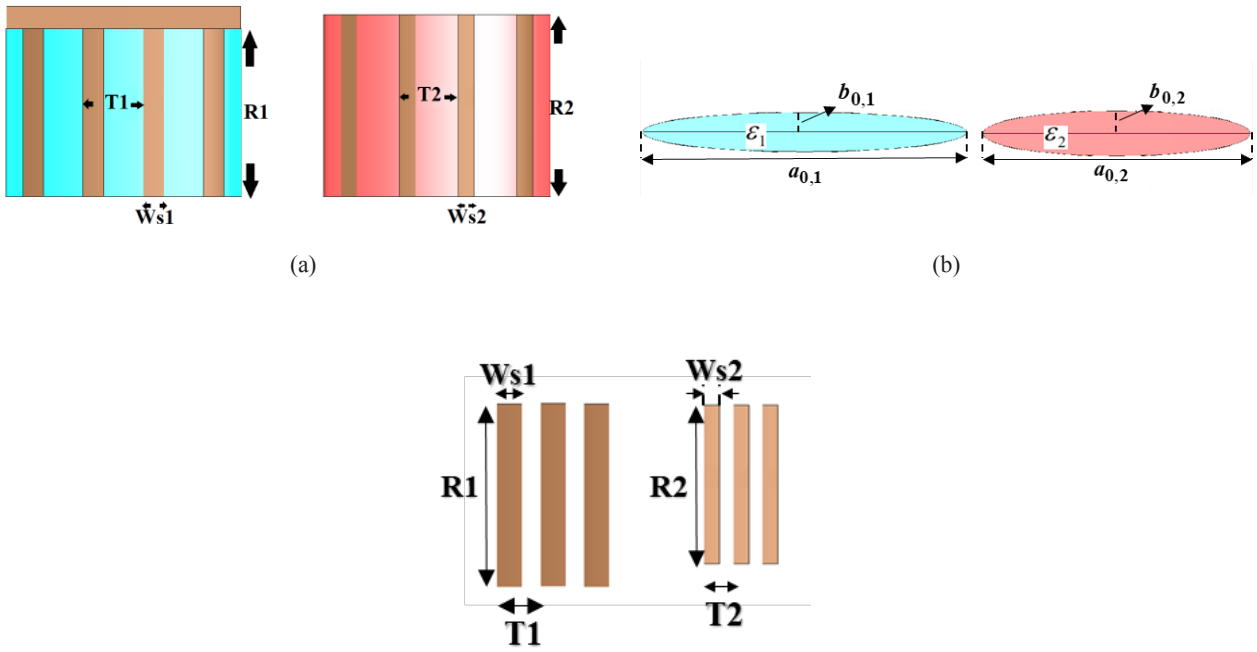

Fig. 8. a) Front view and b) side view of mantle cloaks around the patches, c) parallel metal strips as a metasurface

$$\sigma_{3D} = \sigma_{2D}\frac{2L^2}{\lambda}\sin^2(\theta_s) \times \mathrm{sinc}\left(\frac{k_0 L}{2}(\cos(\theta_i)+\cos(\theta_s))\right) \quad (6)$$

where θ_i and θ_s are the incident and scattering angles, respectively. Here, the incident angle is assumed to be 90° (normal incidence). As seen, the SCS of finite and infinite cylinders differ but are proportional to each other. By reducing the SCS of the infinite cylinder (2D case), we also decrease the SCS of the finite cylinder (3D case). Consequently, the surface reactance (X_s) required to eliminate the scattering of the first mode in the infinite case can be applied to the finite case as well. However, it is important to note that while the analytical optimum value of X_s "completely" cancels the scattering of the first mode in the 2D (infinite) case, only leads to a "partial" reduction of scattering in the 3D (finite) case.

In summary, if the cloak is perfectly tailored to minimize the scattering of an infinite cylinder at a specific frequency, reducing the cylinder's length to a finite size does not change the frequency at which scattering is minimized. Therefore, to avoid the super-complex scattering equations of the finite elliptic cylinder, it is a routine procedure to calculate the design parameters for the infinite case and make minor numerical optimizations to minimize scattering in the finite case.

In this study, the scattering of the electric field in normal incidence is mainly influenced by TM polarization. Therefore, TM illumination is used to determine the optimal X_s of the covering mantle cloak. While the angle of the incident electric field is 90° and the patch antenna is narrowband, the initial values of the cloak parameters obtained from analytical formulas of the infinite cylinder are suitable for reducing scattering in the finite case. Therefore, "extensive" numerical optimization is not required. A minor optimization approach, involving a ±5% change in the parameters around their initial values, effectively decouples the adjacent patches and restores their radiation characteristics to resemble the isolated case. As a result, the design procedure becomes practical and straightforward, eliminating the need for complex calculations to obtain the optimal X_s of finite cylinder cloak, which otherwise would require iterative numerical solutions to the scattering problem [20].

By using the quasi-static approximation, we calculate the optimum surface reactance in a closed-form manner, as Eq. (7), where it is then applied to cancel out the scattering of the metallic elliptic cylinder (patch) covered with a thin dielectric material having a permittivity of ε_r [18]:

$$X_s = \omega\mu F\frac{(u_0-u_1)\cosh u_0}{1+(q_0(u_0-u_1)+q_1(u_1+(1/2)\ln q_1))\sinh 2u_0} \quad (7)$$

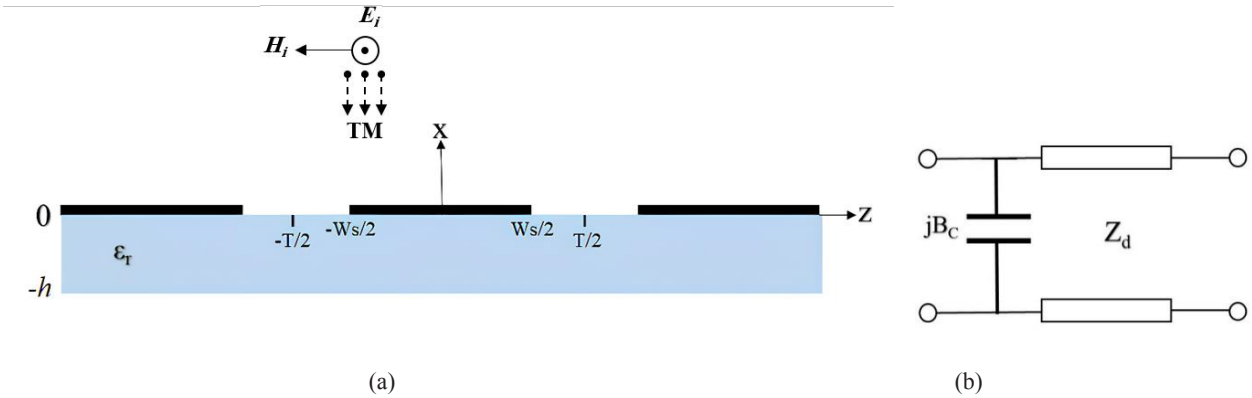

Fig. 9. a) Geometric structure of strip grating on a dielectric substrate and b) equivalent circuit model for metallic strips supported by a dielectric substrate under TM illumination

where $q_0 = k_0^2 F^2 / 4$, $q_1 = k_1^2 F^2 / 4$, and k_0 and k_1 are the wavenumbers in free space and dielectric, respectively. F is the focal length of the ellipse, $u_0 = tanh^{-1}(b_{0,i} / a_{0,i})$, $u_1 = tanh^{-1}(b_{1,i} / a_{1,i})$, $a_{0,i}$ and $b_{0,i}$ are the major and minor diameters of the elliptical dielectric, $a_{1,i}$ and $b_{1,i}$ are the major and minor diameters of the metallic elliptic cylinder, respectively. Here, i = 1, 2 refers to Array I and Array II, respectively. The parameters $a_{1,i}$ and $b_{1,i}$ represent the length and thickness of the patch, respectively, with the thickness tending to zero.

Fig. 6 illustrates the mantle cloaks proposed for both arrays. To counteract the inductive reactance of the dielectric-covered patch (Eq. (7)), we employ 1D conformal sub-wavelength metallic metasurface components, specifically parallel strips as shown in Fig. 8(c). These components are designed to possess the required surface capacitive reactance, which is equal to Eq. (7). To determine the capacitive reactance of these strips, we utilize the equivalent circuit model method.

The periodic structure of strips on a low-loss dielectric layer can be represented by an equivalent shunt susceptance cascaded with a transmission line, as shown in Fig. 9. The transmission line has a characteristic impedance (Z_d) that corresponds to the wave impedance within the dielectric layer, and its length represents the thickness of the dielectric substrate. The value of the susceptance (B_C) is determined by the characteristics of the strips (width and periodicity) and the substrate (thickness and dielectric constant). It is important to account for the effects of the dielectric substrate on the shunt susceptance. According to Fig. 9(a), the metal strips with a width of "Ws" and zero thickness, are uniformly spaced with a periodicity of "T" on the dielectric substrate. Fig. 9(b) illustrates its equivalent circuit model when illuminated by TM waves.

An approximate calculation can be employed to determine the normalized equivalent shunt capacitive susceptance [21]:

$$B_C = B_{C0}\{1+[0.4635(\varepsilon_r - 1) + 0.0091(\varepsilon_r - 1)^2]C_d\left(\frac{Ws}{T}, \frac{T}{\lambda}\right)(1 - e^{1.8kh})\} \quad (8)$$

where

$$B_{C0} = \frac{k_0 T}{\pi}\left[0.13(\frac{Ws}{\lambda})^2 C_0\left(\frac{Ws}{T}, \frac{T}{\lambda}\right) - \ln(\cos\frac{\pi Ws}{T})\right] \quad (9)$$

$$C_0\left(\frac{Ws}{T}, \frac{T}{\lambda}\right) = \left[1 - \frac{T}{\lambda} - 0.6875(\frac{T}{\lambda})^2\right] \times \left[1 - 0.7174\frac{Ws}{T} + 172.2(\frac{Ws}{T})^2 - 294.2(\frac{Ws}{T})^3\right] \quad (10)$$

$$C_d\left(\frac{Ws}{T}, \frac{T}{\lambda}\right) = 1.255\left[1 - 0.0777\frac{T}{\lambda} - 0.7917(\frac{T}{\lambda})^2\right] \times \left[1 - 1.37\frac{Ws}{T} + 2.1816(\frac{Ws}{T})^2\right] \quad (11)$$

Several analyses are performed to demonstrate the characteristics of the metal strip grating and evaluate the accuracy of the equivalent circuit model. The Equations (8)-(11) used in these analyses are derived by fitting curves to the results obtained from calculations using the spectral domain method. Experimental findings indicate that the equations for TM and TE illuminations exhibit a 99% accuracy when compared to the results obtained from the spectral domain [21].

The long and complex formulation of the equivalent circuit model method makes it difficult to use it accurately. Therefore, the approximate equations outlined in [22] are preferred. Although this alternative approach is not as precise,

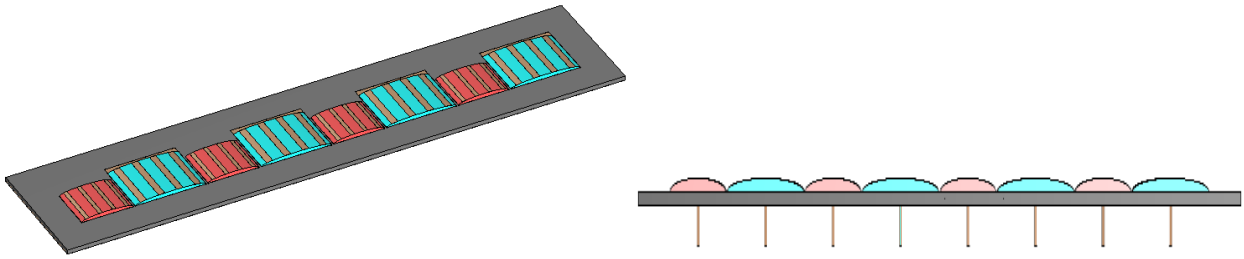

(a) (b)

Fig. 10. a) 3D view and b) side view of the cloaked arrays

Table 2. Design parameters of mantle cloaks

Parameter	Ws1	Ws2	R1	R2	T1	T2	$a_{0,1}$
Value (mm)	0.27	0.17	2.24	1.85	0.8	0.59	3.13
Parameter	$a_{0,2}$	$a_{1,1}$	$a_{1,2}$	$b_{0,1}$	$b_{0,2}$	$b_{1,1}$	$b_{1,2}$
Value (mm)	2.3	3.11	2.27	0.19	0.19	0	0

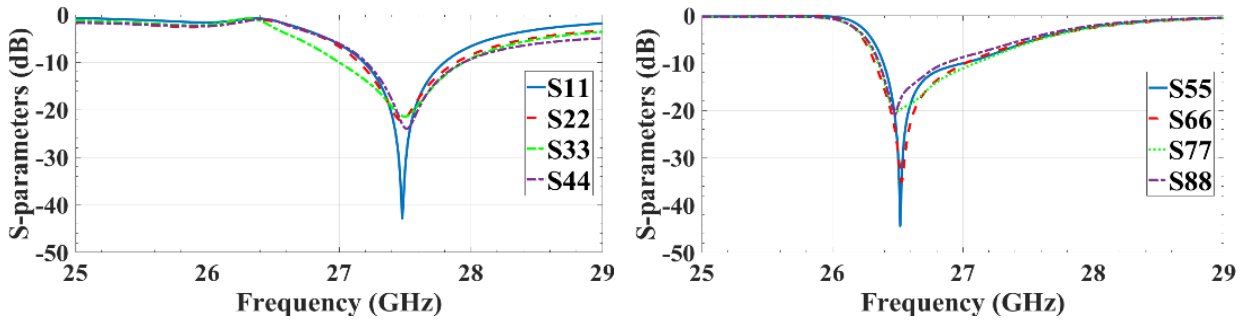

(a) (b)

Fig. 11. Reflection coefficients of elements in the interleaved cloaked configuration. a) Array I, b) Array II

it still yields good accuracy and speeds up the design and calculation process of the cloak [23].

To determine the surface reactance of the conformal metasurface elements in the quasi-static approximation, we employ the analytical grid-impedance expression, which can be expressed as follows [22]:

$$Z_s = -j\frac{\omega\eta_0 T}{4c\pi}\ln\csc\left(\frac{\pi W s}{2T}\right) \quad (12)$$

Eq. (12) simplifies the design process while maintaining an acceptable level of accuracy. The magnitude of the capacitive reactance of Eq. (12) must be equal to the surface inductive reactance of Eq. (7), to effectively eliminate coupling between patch array antennas.

2- 2- Characteristics of the patch arrays in the cloaked case

Fig. 10 shows the elements of tightly spaced interleaved arrays covered by mantle cloaks. The design parameters of the mantle cloaks are summarized in Table 2.

In Fig. 11, the reflection coefficients of two cloaked arrays are shown, indicating that impedance matching is restored for both arrays. These results closely resemble those observed in the isolated case depicted in Fig. 2. Additionally, Fig. 12 demonstrates the mutual coupling between the central elements of two arrays in an interleaved cloaked configuration. It is evident that the cloak has effectively

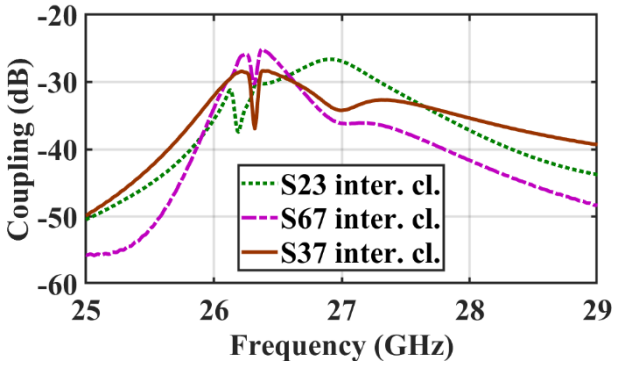

Fig. 12. Mutual coupling between the central elements of two arrays in interleaved cloaked configuration.

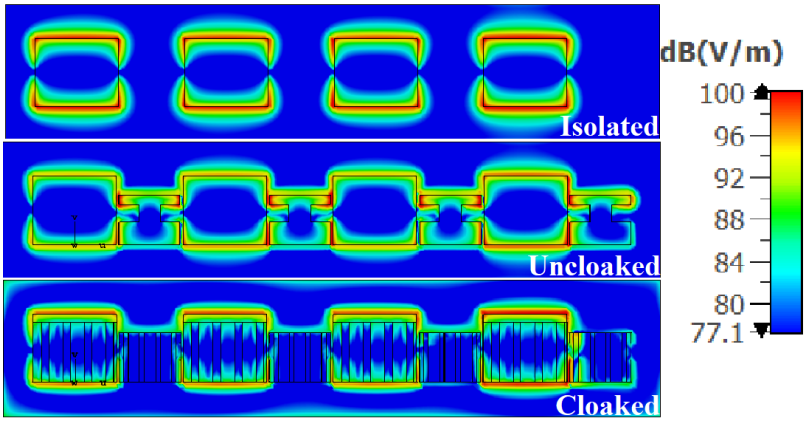

(a)

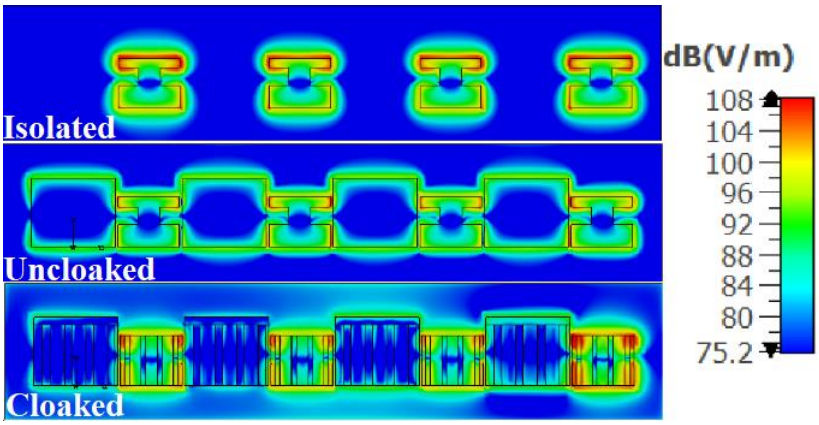

(b)

Fig. 13. E-field distribution for three cases when a) Array I is excited and Array II is matched, b) Array II is excited and Array I is matched

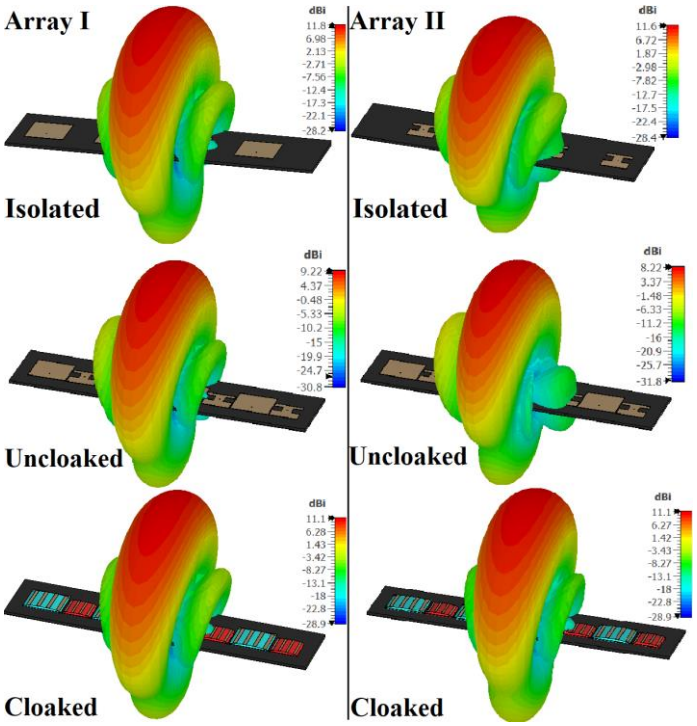

Fig. 14. Comparison between the 3D gain patterns of the two arrays in three configurations

eliminated the mutual coupling between the elements, resulting in over 10 dB improved isolation compared to the uncloaked case shown in Fig. 4.

Fig. 13 shows the E-field distributions of two arrays at their respective operating frequencies. In Fig. 13(a), Array I elements are excited while Array II elements are matched. Conversely, in Fig. 13(b), Array II elements are excited and Array I elements are matched. In the uncloaked case, a strong coupling between adjacent patches is observed, affecting the E-field distribution of the excited patches. However, this coupling is eliminated when cloaking is applied, resulting in an E-field distribution similar to that of isolated arrays.

According to the analysis of the E-field distribution, when both arrays are excited simultaneously, the cloaked structure shows a maximum E-filed intensity of 17.8 V/mil when it is exposed to an input power of 1 watt. Considering that the breakdown of the resin dielectric material occurs at around 500 V/mil, it can be concluded that each array element can withstand a maximum power of approximately 780 W.

2- 3- Comparison between radiation performance of arrays

In Fig. 14, the 3D radiation patterns of the arrays are compared in three investigated configurations, i.e. isolated, interleaved uncloaked, and interleaved cloaked.

In the cloaked case, a gain increment of 1.9 dB and 2.9 dB, as well as an SLL improvement of 3.4 dB and 5.1 dB are observed for Arrays I and Array II, respectively, compared to the uncloaked case. Moreover, the radiation patterns in the cloaked case closely resembled those of isolated arrays with a similarity of 98% which is calculated using the Pearson Correlation Method (PCM).

Additionally, in Fig. 15 and Fig. 16, a comparison is made between the co-pol and cross-pol (XP) components of the radiation patterns of both arrays, respectively. This comparison is done in the isolated, uncloaked, and cloaked cases at their operating frequencies. It is clear that the radiation patterns of the cloaked arrays closely resemble those of the isolated arrays. Therefore, the proposed mantle cloaks have successfully eliminated the coupling between the two arrays, ensuring that their close proximity does not negatively impact the pattern shape.

In the uncloaked case, the close spacing of the two arrays leads to a strong coupling between them, resulting in an increase of the XP level by approximately 20 dB, as shown in Fig. 16. However, by implementing mantle cloaking on the antennas, the XP level of both arrays is significantly improved and is approximately 40 dB lower than the co-pol component, similar to the isolated arrays.

In addition, Fig. 17 presents a comparison between the efficiencies of two arrays. The results are normalized to the ideal scenario where both arrays radiate separately (isolated case). The findings indicate a significant decrease in efficiency for the uncloaked case. However, in the cloaked case, the

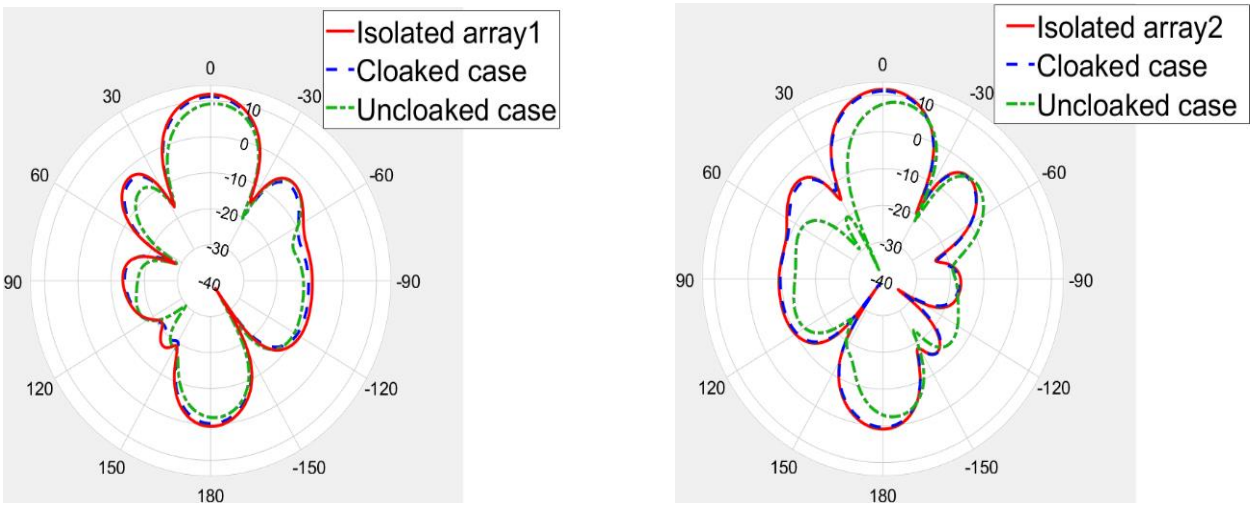

(a) (b)

Fig. 15. Comparison between the co-pol components of the radiation patterns of the antennas at their operating frequencies in three cases in φ = 0° plane. a) Array I, b) Array II

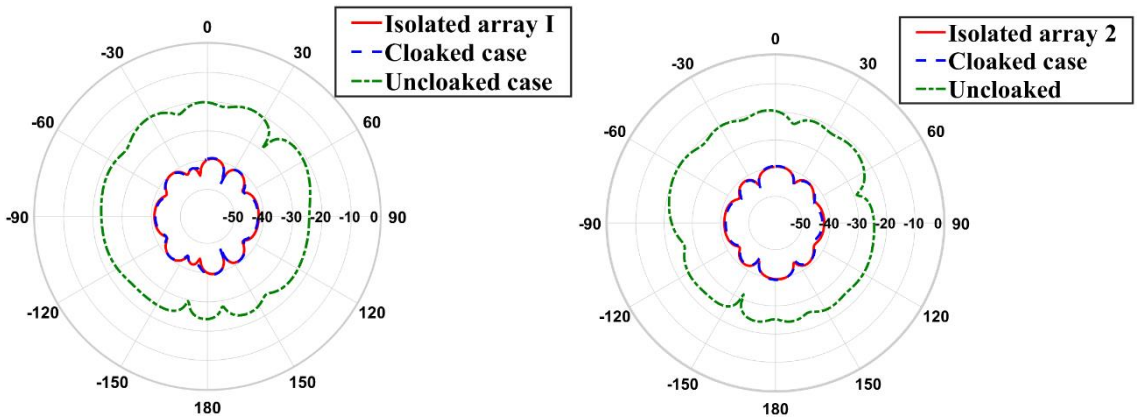

(a) (b)

Fig. 16. Comparison between the cross-pol components of the radiation patterns of the antennas at their operating frequencies in φ = 90° plane. a) Array I, b) Array II

efficiency is nearly fully restored and reaches approximately 97%.

In Table 3, the peak gain, side lobe level (SLL), and efficiency of three cases are compared for Array I and Array II.

2- 4- Beam steering performance of arrays

In the phased arrays, to ensure full-range beam steering without grating lobe appearance, it is crucial to maintain a maximum spacing of $\lambda/2$ between the elements. This requirement has been met in this design by incorporating slots on the edges of the patches of Array II and reducing their dimensions. By uniformly exciting the elements with different phases, the main beam of the radiation pattern is rotated to scan the space. The inclusion of the cloaks around the patches does not impact the beam steering capability of the arrays.

Fig. 18(a) and 18(b) illustrate the radiation patterns of both arrays, with the beam rotated within the range of ±30°. The

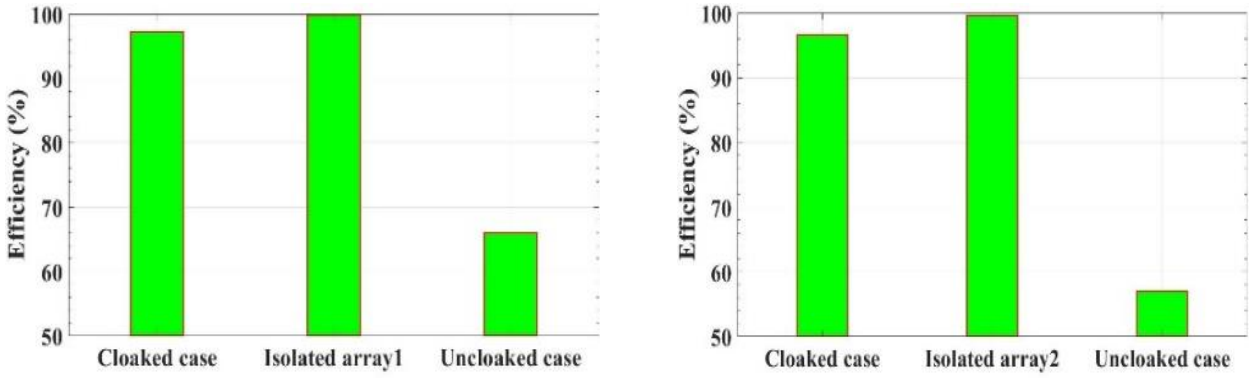

(a) (b)

Fig. 17. Comparison between the efficiencies of three cases normalized to the isolated case. a) Array I, b) Array II

Table 3. Comparison between the radiation characteristics of the arrays in the isolated, uncloaked and cloaked cases

Cases		Isolated	Uncloaked	Cloaked
Array I	Gain (dB)	11.7	9.2	11.1
	SLL (dB)	13.8	9.7	13.1
	Normalized Efficiency (%)	100	97	66
Array II	Gain (dB)	11.6	8.2	11.1
	SLL (dB)	13.1	8	13.1
	Normalized Efficiency (%)	100	97	57

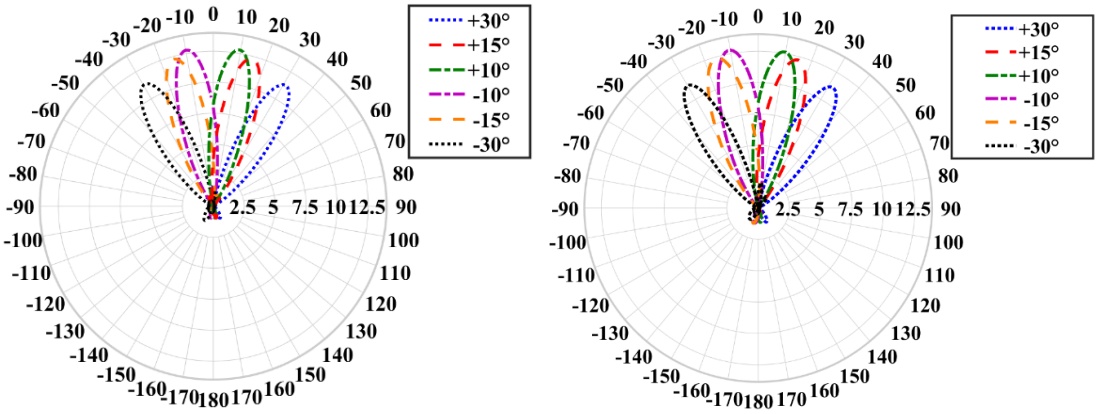

(a) (b)

Fig. 18. Beam steering performance of a) Array I, b) Array II

Table 4. Comparison of decoupling methods used in the literature with the current study.

Characteristic / Ref.	Method of decoupling	Edge to edge Element Spacing	Complexity of the decoupling method	Decoupling level (dB)	Frequency (GHz)	Antenna type
[23]	Mantle Cloaking (for antennas with orthogonal polarizations)	0.012 λ_0	Low with an almost planar structure	24	3.7	Patch
[24]	Ceramic superstrate-based decoupling method	0.28 λ_0	Medium with 3D structure	25	3.5	Dipole
[25]	Central-symmetry decoupling technique	0.11 λ_0	Low	22	2.5	Patch
[26]	Mixed radiation modes	0.11 λ_0	Medium with 3D structure	23	2.5	Patch
[27]	Decoupling dielectric stubs	0.27 λ_0	Medium with 3D structure	20	4.75	Patch
[28]	Frequency-selective surface (FSS)	0.22 λ_0	Medium with 3D structure	18	4	Patch
[29]	High-impedance electromagnetic structure (HIES) and Artificial magnetic conductor (AMC)	0.15 λ_0	Medium with 3D structure	27	4.3	Patch
[30]	Artificial magnetic conductor (AMC)	0.32 λ_0	High with a 3D multilayer structure	28	6.25	Patch
This work	**Mantle cloaking (for antennas with the same polarization and close frequencies)**	**0.01 λ_0**	**Low with an almost planar structure and beam steering ability**	**26**	**27.5**	**Patch**

patterns are presented in a linear scale to improve clarity and accurately measure the angle of rotation. The sidelobe level (SLL) remains below -10 dB within this steering range, and the gain only decreases by a maximum of 1.5 dB compared to the broadside direction.

3- Discussion

Table 4 presents a comparison between the decoupling techniques of array antennas previously published and the current work. The comparison is based on the spacing between the elements, the complexity of the decoupling method, and the level of decoupling.

This study focuses on developing a cloak specifically designed for an active device, i.e. antenna. The main goal is to replicate the antenna's radiation characteristics as closely as possible when it is isolated. To evaluate the performance of the cloak, the radiation characteristics and scattering parameters are compared between isolated, cloaked, and uncloaked cases. Here, the analysis includes examining return loss, coupling, radiation patterns, gain, and efficiency of the antennas in these three scenarios. The results demonstrate the effectiveness of the proposed approach.

In the proposed configuration, the edge-to-edge spacing between the elements is 0.1 mm ($\lambda/100$), which is significantly smaller than the previous designs. However, this distance is chosen to avoid electrical shorting between the patches and to accommodate manufacturing limitations. In theory, this spacing can be reduced to almost zero because adjacent cloaked patches practically do not "see" each other and are completely isolated.

This study introduces a novel approach to address the limitations of passive cloaks by incorporating anisotropic cloaks. These cloaks effectively eliminate coupling between two co-planar patch array antennas that operate at close

frequencies. By implementing this novel method, it becomes possible to use nearly the same space size that would typically accommodate a single antenna array to place two arrays in very close proximity. This can result in space savings of up to 50% in compact 5G applications with limited spatial availability.

4- Conclusion

We proposed the use of tailored elliptical metasurfaces for mantle cloaking, which can efficiently decouple densely arranged linear co-planar patch arrays. Through the simulations, we have demonstrated that by enclosing the elements of interleaved arrays with appropriate cloaks, the detrimental effects of mutual coupling can be completely eliminated. As a result, the antennas regain their original radiation characteristics, similar to when they operate independently. The application of tailored elliptical metasurfaces for mantle cloaking exhibits significant promise in communication fields, particularly for compact 5G and 6G smartphones. It enables the implementation of tightly spaced antenna arrays, further enhancing the capabilities of these devices.

References

[1] D. Schurig, J.J. Mock, B. Justice, S.A. Cummer, J.B. Pendry, A.F. Starr, D.R. Smith, Metamaterial electromagnetic cloak at microwave frequencies, Science, 314(5801) (2006) 977-980.

[2] A. Alù, Mantle cloak: Invisibility induced by a surface, Physical Review B, 80(24) (2009) 245115.

[3] A. Monti, L. Tenuti, G. Oliveri, A. Alù, A. Massa, A. Toscano, F. Bilotti, Design of multi-layer mantle cloaks, 8th International Congress on Advanced Electromagnetic Materials in Microwaves and Optics, 2014, pp. 214-216.

[4] A. Monti, J.C. Soric, A. Alù, A. Toscano, F. Bilotti, Anisotropic mantle cloaks for TM and TE scattering reduction, IEEE Transactions on Antennas and Propagation, 63(4) (2015) 1775-1788.

[5] A. Monti, J. Soric, M. Barbuto, D. Ramaccia, S. Vellucci, F. Trotta, A. Alu, A. Toscano, F. Bilotti, Mantle cloaking for co-site radio-frequency antennas, Applied Physics Letters, 108(11) (2016) 113502.

[6] G. Moreno, A.B. Yakovlev, H.M. Bernety, D.H. Werner, H. Xin, A. Monti, F. Bilotti, A. Alù, Wideband elliptical metasurface cloaks in printed antenna technology, IEEE Transactions on Antennas and Propagation, 66(7) (2018) 3512-3525.

[7] A. Monti, J. Soric, A. Alù, A. Toscano, F. Bilotti, Design of cloaked Yagi-Uda antennas, EPJ Applied Metamaterials, 3 (2016) 10.

[8] S. Vellucci, A. Monti, M. Barbuto, M. Salucci, G. Oliveri, A. Toscano, F. Bilotti, Non-linear mantle cloaks for self-configurable power-dependent phased arrays, XXXIIIrd General Assembly and Scientific Symposium of the International Union of Radio Science, IEEE, 2020, pp. 1-3.

[9] S. Vellucci, A. Monti, M. Barbuto, M. Salucci, G. Oliveri, A. Toscano, F. Bilotti, Overcoming mantle cloaking limits in antenna applications through non-linear metasurfaces, Fourteenth International Congress on Artificial Materials for Novel Wave Phenomena (Metamaterials), IEEE, 2020, pp. 355-357.

[10] S. Vellucci, A. Monti, M. Barbuto, G. Oliveri, M. Salucci, A. Toscano, F. Bilotti, On the use of nonlinear metasurfaces for circumventing fundamental limits of mantle cloaking for antennas, IEEE Transactions on Antennas and Propagation, 69(8) (2021) 5048-5053.

[11] S. Vellucci, A. Monti, M. Barbuto, A. Toscano, F. Bilotti, Waveform-selective mantle cloaks for intelligent antennas, IEEE Transactions on Antennas and Propagation, 68(3) (2019) 1717-1725.

[12] S. Vellucci, A. Monti, M. Barbuto, A. Toscano, F. Bilotti, Progress and perspective on advanced cloaking metasurfaces: from invisibility to intelligent antennas, EPJ Applied Metamaterials, 8 (2021) 7.

[13] X.b. Sun, M.Y. Cao, Low mutual coupling antenna array for WLAN application, Electronics Letters, 53(6) (2017) 368-370.

[14] K.S. Vishvaksenan, K. Mithra, R. Kalaiarasan, K.S. Raj, Mutual coupling reduction in microstrip patch antenna arrays using parallel coupled-line resonators, IEEE Antennas and Wireless Propagation Letters, 16 (2017) 2146-2149.

[15] Q. Li, A.P. Feresidis, M. Mavridou, P.S. Hall, Miniaturized double-layer EBG structures for broadband mutual coupling reduction between UWB monopoles, IEEE Transactions on Antennas and Propagation, 63(3) (2015) 1168-1171.

[16] Y.-F. Cheng, X. Ding, W. Shao, B.Z. Wang, Reduction of mutual coupling between patch antennas using a polarization-conversion isolator, IEEE Antennas and Wireless Propagation Letters, 16 (2016) 1257-1260.

[17] A.K. Panda, S. Sahu, R.K. Mishra, A compact dual-band 2× 1 metamaterial inspired mimo antenna system with high port isolation for LTE and WiMax applications, International Journal of RF and Microwave Computer-Aided Engineering, 27(8) (2017) e21122.

[18] H.M. Bernety, A.B. Yakovlev, Cloaking of single and multiple elliptical cylinders and strips with confocal elliptical nanostructured graphene metasurface, Journal of Physics: Condensed Matter, 27(18) (2015) 185304.

[19] A. Moosaei and M.H. Neshati, Design investigation of mantle-cloak for a PEC cylindrical object under oblique incidence of TM and TE waves, AEU-International Journal of Electronics and Communications, 1(137) (2021) 153801.

[20] J.H. Richmond, Scattering by a conducting elliptic cylinder with dielectric coating, Radio Science, 23(06) (1988) 1061-1066.

[21] W. Wang, Y. Guo, Analysis of metal grating polarizers for quasi-optical power combining applications, International journal of infrared and millimeter waves,

16 (1995) 123-133.

[22] Y.R. Padooru, A.B. Yakovlev, P.Y. Chen, A. Alu, Analytical modeling of conformal mantle cloaks for cylindrical objects using sub-wavelength printed and slotted arrays, Journal of Applied Physics, 112(3) (2012) 034907.

[23] R. Masoumi, R. Kazemi, A.E. Fathy, Design and implementation of elliptical mantle cloaks for polarization decoupling of two tightly spaced interleaved co-frequency patch array antennas, Scientific Reports, 13(1) (2023) 2885.

[24] F. Liu, J. Guo, L. Zhao, G.L. Huang, Y. Li, and Y. Yin, Ceramic superstrate-based decoupling method for two closely packed antennas with cross-polarization suppression, IEEE Transactions on Antennas and Propagation, 69(3) (2020) 1751-1756.

[25] K.L. Chung, A. Cui, M. Ma, B. Feng, and Y. Li, Central-Symmetry decoupling technique for circularly-polarized MIMO system of tightly packed Chinese-character shaped patch antennas, The Applied Computational Electromagnetics Society Journal (ACES), (2021) 1125-1131.

[26] Y.F. Cheng and K.K.M. Cheng, Decoupling of 2× 2 MIMO antenna by using mixed radiation modes and novel patch element design, IEEE Transactions on Antennas and Propagation, 69(12) (2021) 8204-8213.

[27] P. Mei, Y. M. Zhang, and S. Zhang, Decoupling of a wideband dual-polarized large-scale antenna array with dielectric stubs, IEEE Transactions on Vehicular Technology, 70(8) (2021), 7363-7374.

[28] R. Qi, D. Yang, H. Zhai, Y. Zeng, and Z. Wang, Patch antenna array decoupling based on polarization conversion frequency selective surface, International Conference on Microwave and Millimeter Wave Technology (ICMMT), (2020) 1-3.

[29] A. Abbas, M. Elsaid, S.F. Mahmoud, E.A. Abdallah, and H.M. El-Hennawy, Decoupling of closely stacked patch antennas for airborne radio altimeter applications, AEU-International Journal of Electronics and Communications, 128 (2021) 153506.

[30] H. Malekpoor, A. Abolmasoumi, and M. Hamidkhani, High gain, high isolation, and low-profile two-element MIMO array loaded by the Giuseppe Peano AMC reflector for wireless communication systems, IET Microwaves, Antennas & Propagation, 16(1) (2022) 46-61.

HOW TO CITE THIS ARTICLE

R. Masoumi, R. Kazemi, Exploring the Potential of Elliptical Metasurfaces for Decoupling and Cloaking of Tightly Spaced and Interleaved Patch Array Antennas in 5G Applications, AUT J Electr Eng, 55(2) (2023) 145-160.

DOI: 10.22060/eej.2023.22529.5547